AGU PUBLICATIONS

JGR

Journal of Geophysical Research: Space Physics

RESEARCH ARTICLE
10.1002/2014JA019960

Key Points:
- IRI-2012 and NeQuick2 models are validated using GPS TEC measurements
- The modeled TEC has shown improved performance during low solar activity
- The EIA strength is underestimated by the models in increased solar activity

Correspondence to:
K. Venkatesh,
venkatkau@gmail.com

Citation:
Venkatesh, K., P. R. Fagundes, G. K. Seemala, R. de Jesus, A. J. de Abreu, and V. G. Pillat (2014), On the performance of the IRI-2012 and NeQuick2 models during the increasing phase of the unusual 24th solar cycle in the Brazilian equatorial and low-latitude sectors, *J. Geophys. Res. Space Physics*, *119*, 5087–5105, doi:10.1002/2014JA019960.

Received 10 MAR 2014
Accepted 4 JUN 2014
Accepted article online 10 JUN 2014
Published online 27 JUN 2014

On the performance of the IRI-2012 and NeQuick2 models during the increasing phase of the unusual 24th solar cycle in the Brazilian equatorial and low-latitude sectors

K. Venkatesh[1], P. R. Fagundes[1], Gopi K. Seemala[2], R. de Jesus[1], A. J. de Abreu[1], and V. G. Pillat[1]

[1]Universidade do Vale do Paraiba, IP&D, Sao Jose dos Campos, Brazil, [2]Indian Institute of Geomagnetism, Navi Mumbai, India

Abstract It is known that the equatorial and low-latitude ionosphere is characterized with typical dynamical phenomena namely, the equatorial ionization anomaly (EIA). Accurate modeling of the characteristic variations of the EIA is more important to arrive at the correct estimation of range delays required for the communication and navigation applications. The total electron content (TEC) data from a chain of Global Positioning System (GPS) receivers at seven identified locations from equator to the anomaly crest and beyond along 315°E geographic longitude in the Brazilian sector are considered. The performances of the latest available IRI-2012 and NeQuick2 models have been investigated during 2010–2013 in the increasing phase of the 24th solar cycle. A comparative study on the morphological variations of the GPS measured and modeled TEC revealed that the performances of the models are improved during low solar activity periods compared to that during the increased solar activity years. The strength and the locations of the EIA crest are nearly well represented by both the models during the low solar activity while the models underestimate the peak TEC at the EIA during the increased solar activity conditions. The deviations between the GPS-measured and model-derived TEC are more during equinoctial and summer months at and around the anomaly crest locations. Significant differences have also been observed in between the TEC values derived from both the models. The causes for the discrepancies in the modeled TEC values are discussed based on the model-derived and ionosonde-measured vertical electron density profiles variations.

1. Introduction

The total electron content (TEC) is an important parameter of the ionosphere and plays a vital role in the determination of range delays required for the satellite-based communication and navigation applications. The morphological features of TEC such as the diurnal, seasonal, latitudinal, and solar activity variations have been investigated by several workers using various techniques over different parts of the globe [*Lanyi and Roth*, 1988; *Goodwin et al*., 1995; *Abdu et al*., 1996; *Davies and Hartman*, 1997; *Mannucci et al*., 1998; *Afraimovich et al*., 2001; *Brunini et al*., 2003; *Jee et al*., 2005; *Rama Rao et al*., 2006; *Bagiya Mala et al*., 2009; *Prasad et al*., 2012]. One of the most important electrodynamical features of the equatorial ionosphere is the double-humped latitudinal distribution of ionization centered at the dip equator, which is popularly known as the equatorial ionization anomaly (EIA) [*Appleton*, 1946]. Under the influence of the equatorial fountain effect in the presence of mutually perpendicular electric and magnetic fields, the plasma over the equator is lifted to the higher altitudes and diffuses along the magnetic field lines under the gravitational and pressure gradient forces. As a consequence, the plasma is redistributed forming two ionization crests on either sides of the equator around ±20° latitudes with a trough over the equator. In the presence of the well-developed EIA, the TEC varies significantly in space and time with large latitudinal as well as the altitudinal gradients. A detailed understanding on the characteristics of the ionization anomaly crest such as the strength, location, and local time of the formation of the anomaly crest is more essential to understand the TEC variability. With the increased demand for the satellite-based communication and navigation system applications, modeling the ionospheric TEC has gained more importance. Particularly, in the equatorial and low latitudes, the estimation of the true value of TEC has become a challenging task in view of the large spatiotemporal gradients in the presence of the EIA. In the presence of these gradients, the estimation of TEC poses another problem owing to the mapping function while converting the slant TEC (STEC) to vertical TEC (VTEC) and vice versa for navigation applications. Therefore, it is very much needed to estimate the strength

and location of the anomaly crest with less error to arrive at the accurate modeling of the total electron content and corresponding range delays over the equatorial and low latitude sectors.

Among different models that have been developed for many decades to understand the variations of the ionospheric parameters, the International Reference Ionosphere (IRI) and NeQuick are most widely used empirical models for the estimation of ionospheric electron densities. The IRI model is developed for the specification of ionospheric parameters supported by the Committee on Space Research and the International Union of Radio Science (URSI) and it is continuously being improved by a team of international experts as the new data become available. For a given location, time, and date, the IRI model describes the electron density, temperature, composition, and TEC. The first widely circulated edition of this model was IRI-78 [*Rawer et al*., 1978] and several updated versions were released in the later years [*Bilitza*, 1986, 1990, 2001; *Bilitza and Reinisch*, 2008]. The latest available version of this model is IRI-2012 [*Bilitza et al*., 2014] with significant improvements in estimating the electron density as well as the electron temperature and ion composition. Comparative studies between the experimentally measured and IRI model-derived TEC have been carried out by several workers over different regions of the globe during different solar activity conditions [*Abdu et al*., 1996; *Batista et al*., 1994; *Bhuyan and Borah*, 2007; *Bilitza et al*., 1998; *Prasad et al*., 2012]. A detailed study using the IRI model in the Northern Hemisphere for low-, midlatitude, and high-latitude sectors revealed that the IRI is capable of reproducing the observed TEC well in high latitudes and midlatitudes but failed at low latitudes [*McNamara*, 1984, 1985]. Several comparative studies using different versions of the IRI model have also reported discrepancies in the estimation of the electron density over equatorial and low latitudes [*Bhuyan and Borah*, 2007; *Luhr and Xiong*, 2010; *Sethi et al*., 2011; *Venkatesh et al*., 2011; *Olwendo et al*., 2013].

The NeQuick model is a time-dependent three-dimensional ionospheric electron density model, now available in its version 2 [*Nava et al*., 2008]. This latest version of NeQuick is able to provide TEC in vertical and along different slant paths. This model can also provide TEC along the raypath from a satellite to an Earth station. The NeQuick is a quick run model which has also been adopted by the International Telecommunication Union for TEC modeling [*International Telecommunication Union*, 2003]. The NeQuick model uses a sum of five semi-Epstein layers for the bottomside ionosphere upto the F_2 layer peak and the sixth semi-Epstein layer to describe the topside ionosphere [*Rawer*, 1982]. The NeQuick model has also been validated by several workers and reported good agreement over the middle latitudes and improved performance while assisted by measurements [*Jodogne et al*., 2004; *Bidaine and Warnant*, 2010]. *Nigussie et al.* [2013] validated the NeQuick2 model over the African low-latitude sector and reported that the NeQuick model shows good agreement during the medium solar activity conditions compared to the low solar activity conditions. However, it is essential to validate the models in view of predicting the characteristic variations of the EIA crest during different solar activity conditions to improve the performance of these models in estimating the accurate electron density over the equatorial and low-latitude sectors. Therefore, the present study is aimed to investigate the performance of the latest versions, the IRI-2012 and NeQuick2 models in predicting the strength and location of the ionization anomaly crest during the increasing phase of the 24th solar cycle.

The 24th solar cycle is associated with several unique features such as the deep and longer solar minimum than it has been expected between the solar cycles 23 and 24. The intensity of the 24th solar maximum is much lower which is going to be the smallest in the past hundred years. Thus, it has become a special interest for the ionospheric research community to understand the variabilities of the ionosphere and performance of the models during this 24th solar cycle. The GPS TEC data over seven different locations from equator to the anomaly crest and beyond in the Brazilian sector during the increasing phase of the 24th solar cycle from 2010 to 2013 have been used to validate the performance of the latest models IRI-2012 and NeQuick2. Further, case studies are described to compare the model-derived vertical electron density profiles with the ionosonde-derived bottomside electron density profiles to understand the causes for the discrepancies in the model-derived TEC values.

2. Database

In the recent times, the establishment and development of global as well as different regional GPS receiver networks for ionospheric studies are growing evolutionarily. Thus, the measurements of TEC using the dual

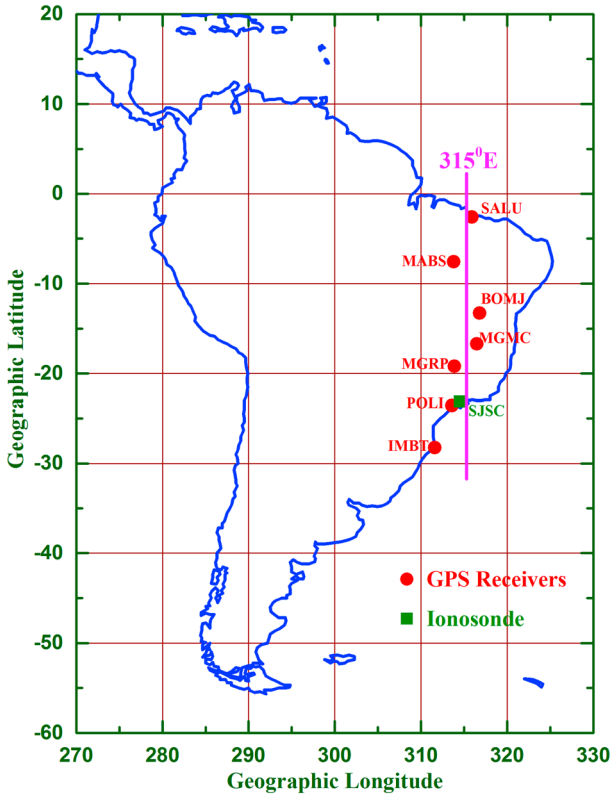

Figure 1. Locations of the GPS receivers from equator to the EIA crest and beyond along the common longitude of 315°E in the Brazilian sector and ionosonde receiver over Sao Jose dos Campos considered for the present study.

frequency GPS receivers have become very efficient database for understanding the different aspects of the ionospheric dynamics with simultaneous and continuous measurements from different regions over the globe. In the present study, the TEC data from a chain of seven identified GPS receivers deployed from equator to the anomaly crest and beyond along the common meridian of 315°E in the Brazilian sector have been considered. The TEC data from these seven stations are downloaded from the database of the Instituto Brasileiro de Geografia e Estatistica (IBGE) network of GPS receivers (http://www.ibge.gov.br/home/geociencias/geodesia/rbmc/rbmc_est.php). The locations of these receivers are shown in Figure 1 and the detailed coordinates are provided in Table 1. The GPS TEC measurements for a 4 year period during the increasing phase of the unusual 24th solar cycle from 2010 (annual mean sunspot number (Rz) = 16) to 2013 (annual mean sunspot number (Rz) = 65) have been used. The dual frequency GPS receivers use two frequencies, L_1 (1575.42 MHz) and L_2 (1227.60 MHz) to derive TEC using differential delay technique. The ionospheric time delay at the L_1 carrier frequency of f_1 as given by *Klobuchar* [1996] is

$$t_1 = 40.3 \times \left(\frac{\mathrm{TEC}}{C.\,f_1^2}\right) \tag{1}$$

where C is the speed of light. The difference in the time delay between L_1 and L_2 frequencies, $\Delta t = t_2 - t_1$ is given by

$$\Delta t = \left(\frac{40.3}{C}\right) \times \frac{\mathrm{TEC}}{\left[\left(1/f_1^2\right) - \left(1/f_2^2\right)\right]} \tag{2}$$

Table 1. Coordinates of the IBGE GPS Receivers and Ionosonde Considered in the Present Study

Sl.No.	Station	Geographic Latitude (°S)	Dip Latitude (°S)	Geographic Longitude (°E)
1	Sao Luis (SALU)	2.59	2.8	315.9
2	Balsas (MABS)	7.53	7.2	313.8
3	Bom Jesus da Lapa (BOMJ)	13.26	12.2	316.8
4	Montes Claros (MGMC)	16.72	15.1	316.5
5	Rio Paranaiba (MGRP)	19.21	17.1	313.9
6	Sao Paulo (POLI)	23.56	20.3	313.6
7	Imbituba (IMBT)	28.23	23.5	311.6
8	Sao Jose dos Compos (SJSC) (Ionosonde)	23.12	20.0	314.5

The slant TEC (STEC) derived using the above relations will produce a noisy result but absolute measurements, while the differential carrier phase gives a precise measure of the relative TEC variations. Therefore, the accuracy of absolute TEC measurements can be improved with the combination of differential phase measurements [*Davies and Hartman*, 1997; *Hocke and Pavelyev*, 2001]. The vertical TEC (VTEC) is given by

$$\mathrm{VTEC} = [\mathrm{STEC} - (b_r + b_s)]/S(E) \tag{3}$$

where b_R is the receiver bias and b_S is the satellite bias. The satellite biases are obtained from those published by the University of Bern and the receiver biases are calculated by minimizing the TEC variability between 0200 and 0600 LT [*Valladares et al.*, 2009; *Seemala and Valladares*, 2011]. The mapping function $S(E)$ is defined as [*Mannucci et al.*, 1993 and *Langley et al.*, 2002]

$$S(E) = \frac{1}{\cos(z)} = \left\{1 - \left(\frac{R_E \times \cos(E)}{R_E + h_s}\right)^2\right\}^{-0.5} \tag{4}$$

where z is zenith angle of the satellite as seen from the observing station, R_E is the radius of the Earth, E is the elevation angle, and h_s is the ionospheric effective height above the Earth's surface which is taken as 350 km [*Rama Rao et al.*, 2006, and references therein].

The simultaneous TEC data from the IRI-2012 and NeQuick2 models have been derived for the seven locations during the considered period from 2010 to 2013. In the IRI-2012 model, the recommended default options "ABT-2009" for bottomside thickness, "NeQuick" for topside electron density profiles, and "URSI" for F layer peak parameters model have been considered. The 10.7 cm solar flux ($F_{10.7}$) is given as the input for both the models. Further, the ionosonde data over a typical anomaly crest location, Sao Jose dos Campos (23.1°S, 314°E) are used to derive the bottomside electron density profiles using POLynomial ANalysis programme (POLAN) true height inversion algorithm [*Titheridge*, 1985]. These experimentally derived bottomside profiles are used to validate the model-derived profiles and F layer peak parameters. Further, the bottomside thickness (B_1) and shape (B_0) parameters have been derived using the following relations

$$N(h) = N_m F_2 . \left[\exp\left(-x^{B1}\right)\right] / \cosh(x) \tag{5}$$

$$x = (h_m F_2 - h)/B_0 \tag{6}$$

where N_mF_2 and h_mF_2 are the F layer peak electron density and heights, respectively. These relations are fitted to the bottomside electron density profiles derived from ionosonde to compute the experimental profile parameters. The IRI-2012 model-derived profile parameters are derived by running the web-based model. The bottomside electron density profiles derived from NeQuick2 models have also been fitted with the above functions to compute the profile parameters. The bottomside profile thickness and shape parameters thus derived using ionosonde and models are compared and the results are discussed.

3. Results

3.1. Diurnal, Seasonal, and Solar Activity Variations of TEC From GPS, IRI-2012, and NeQuick2 Models

The monthly mean diurnal variations of TEC from GPS, IRI-2012, and NeQuick2 models are derived for all the seven stations during four typical months of April, October, December, and July of the low solar activity year 2010 representing the autumn equinox, vernal equinox, summer, and winter seasons, respectively, and the results are presented in Figure 2. The blue-colored curves represent the monthly mean diurnal variation of the GPS-measured TEC values, the red-colored curves with triangles represent the IRI-2012 model-derived TEC variations, and the green-colored curves with circles represent the variations of NeQuick2 model-derived TEC. It is clearly seen from all these plots that the diurnal variation of TEC shows a short-lived day minimum between 0500 and 0600 h LT with the day maximum in the afternoon hours which is found to be broad over the equator. The TEC shows higher values during equinoctial and southern summer months compared to those during winter at all the stations. Nighttime maintenance of ionization is observed during equinoctial and summer months from equator to the anomaly crest locations while the nighttime ionization is almost flat at the day minimum level during winter months at all the latitudes. The diurnal variations of TEC derived from the IRI-2012 and NeQuick2 models represent all the above mentioned features with a difference of about 5 to 10 total electron content unit (TECU) (1 TECU = 10^{16} el/m^2)

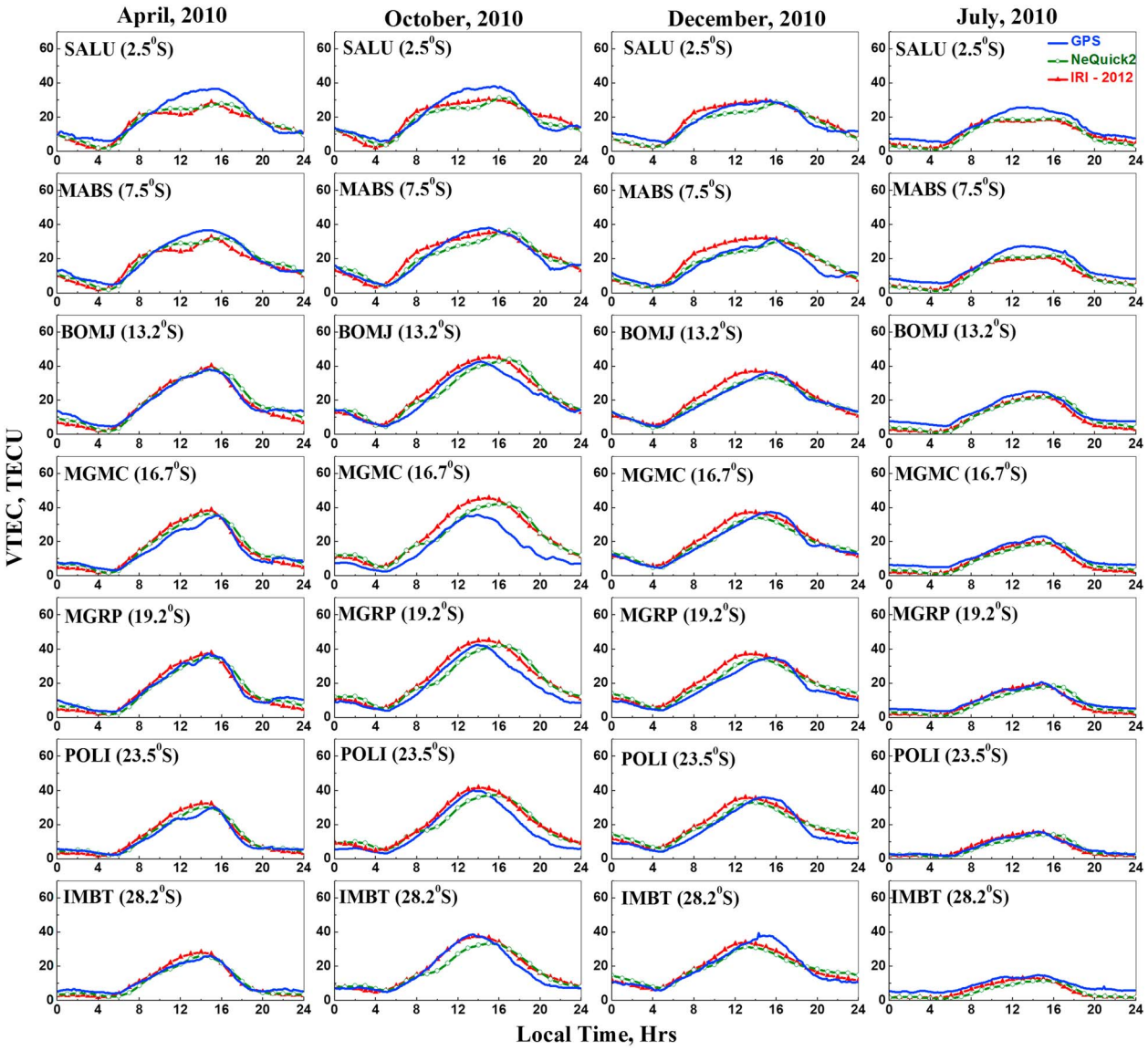

Figure 2. Monthly mean diurnal variation of TEC from GPS (blue curves), IRI-2012 (red curves with triangles), and NeQuick2 (green curves with circles) during April, October, December, and July 2010 representing vernal equinox, autumn equinox, summer, and winter seasons, respectively.

compared to those of the GPS TEC. The model-derived TEC values show more differences during October and December 2010 while they represent good estimation of GPS TEC during April and July 2010 except over the locations SALU and MABS. Significant differences are observed in between the TEC values derived from the two models in the morning hours (from 0600 to 1400 h LT) of the vernal equinox and summer months while the TEC values from these two models is almost similar during autumn and winter months at all the seven different locations. During the southern summer month of December 2010, the TEC from the NeQuick2 model compares well with the GPS-derived TEC while the IRI-2012 model-derived TEC over estimates the GPS TEC in the morning hours between 0600 and 1300 h LT. It is interesting to note that in general, the nighttime TEC values derived from the IRI-2012 and NeQuick2 models compare well with the GPS-derived TEC during the four different seasons at all the locations.

With a view to study the performance of the IRI-2012 and NeQuick2 models during the increased solar activity conditions, the similar analysis has been carried out for the year 2013 for all the stations considered in the present study. The monthly mean diurnal variations of TEC from GPS, IRI-2012, and NeQuick2 models are presented in Figure 3 during April, October, December, and July 2013. It is readily observed from this

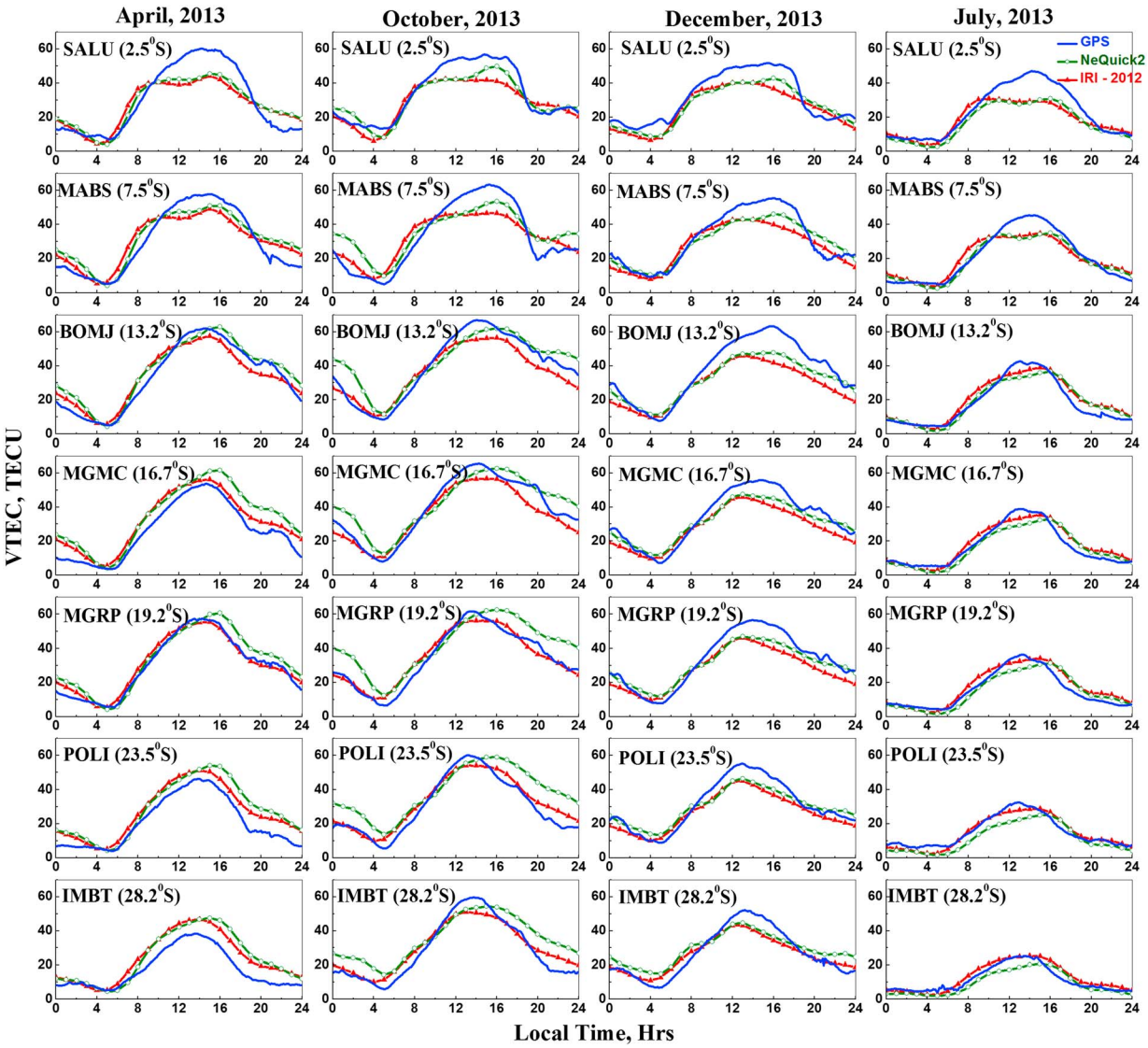

Figure 3. Monthly mean diurnal variations of TEC from GPS (blue curves), IRI-2012 (red curves with triangles), and NeQuick2 (green curves with circles) during April, October, December, and July 2013 representing vernal equinox, autumn equinox, summer, and winter seasons, respectively.

figure that the TEC values are much higher compared to those of the year 2010. The typical features such as the day minimum in the early morning hours, broad day maximum over the equator, and the nighttime maintenance of ionization are more pronounced in the GPS TEC variations. The diurnal variations of TEC from both the models also reflect these features except the nighttime maintenance of ionization at and around the anomaly crest locations. The TEC shows higher values during equinoctial months followed by summer and winter months over the seven different locations. It is seen from these plots that the IRI-2012 and NeQuick2 model-derived TEC values show significant differences as high as 20 TECU compared to the GPS-measured TEC values. These differences are found to be more during the equinoctial months and less during winter months. It is observed, in general, that the model-derived TEC underestimates the GPS TEC during daytime hours and overestimates the GPS TEC during nighttime hours. The nighttime TEC values derived from the NeQuick2 model are much higher showing nearly double than that of GPS TEC values during the vernal equinoctial month of October 2013 particularly at and around the anomaly crest locations. Significant differences have also been observed in between the TEC values derived from the IRI-2012 and NeQuick2 models. During the equinoctial and summer months, the TEC from both the models is nearly similar in the prenoon hours, while in the afternoon and nighttime hours, the NeQuick2-derived

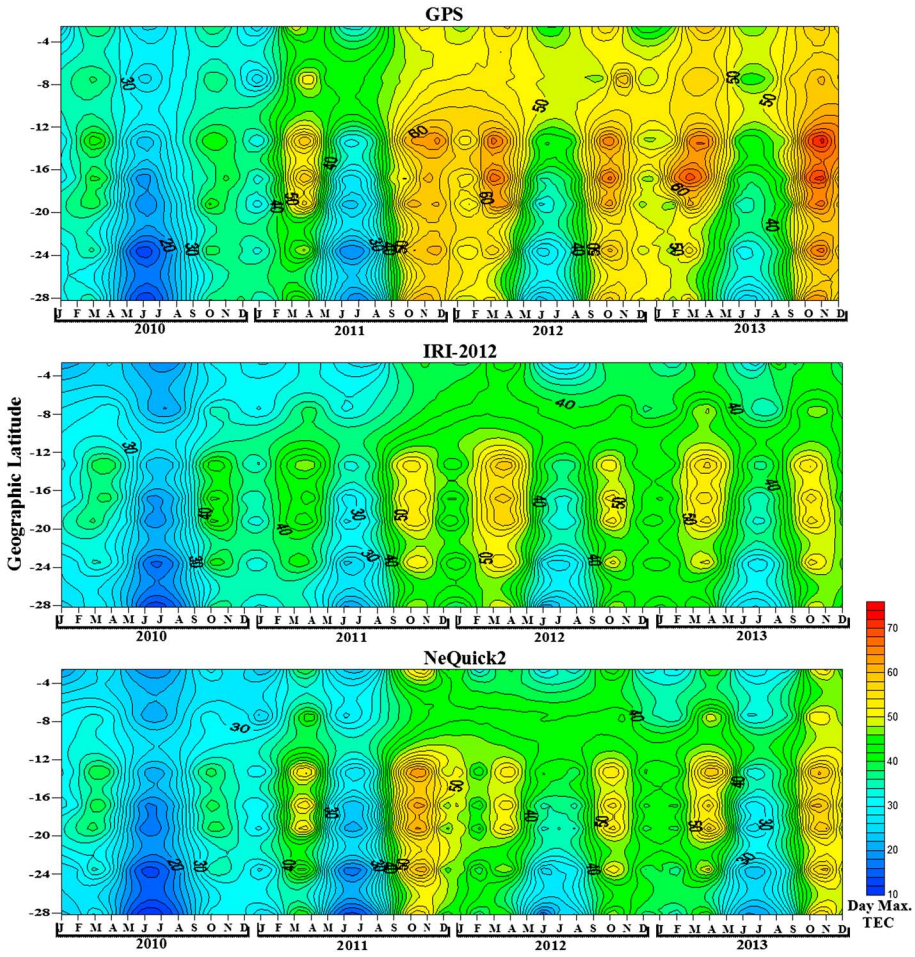

Figure 4. Contour plots showing the variation of day maximum TEC from GPS (top), IRI-2012 (middle) and NeQuick2 (bottom) during a 4 year period from 2010 to 2013 at different latitudes from equator to the EIA crest and beyond.

TEC values are much higher than the IRI-2012 model-derived TEC at all the seven different locations. During the winter month of July 2013, the IRI-2012-derived TEC shows higher values in the prenoon hours while in the afternoon hours, the TEC values from both the models show similar values. The differences in between the IRI-2012 and NeQuick2 model-derived TEC values observed during winter months of the year 2013 are similar to those observed during the equinoctial months of the year 2010.

To study the seasonal and solar activity variations in the experimentally measured and model-derived TEC values, the day maximum TEC values are obtained from the monthly mean diurnal values of TEC for every month during the 4 year period from 2010 to 2013 over all the considered locations. Figure 4 shows the contour plots of the day maximum TEC as a function of latitude and month of the year from January 2010 to December 2013. Figure 4 (top) shows the variation of day maximum TEC from GPS, Figure 4 (middle) shows the variation of day maximum TEC from the IRI-2012 model, and Figure 4 (bottom) shows the day maximum TEC variations from the NeQuick2 model. The semiannual variations in the day maximum values of TEC are clearly observed from GPS and the model-derived TEC values with two peaks around March-April and October-November months of each year. The day maximum TEC values increase from 2010 to 2013 at all the latitudes indicating the solar activity dependence of the TEC, which is also observed in the variations of TEC from the IRI-2012 and NeQuick2 models. Interestingly, during the low solar activity conditions, the magnitude and variations of the day maximum TEC from the IRI-2012 and NeQuick2 models are nearly comparable to those of the GPS-derived TEC. As the solar activity increases toward the year 2013, the TEC values from GPS and both the models also increase. However, during the increased solar activity years, the TEC values from both the models are much lower than those of the GPS

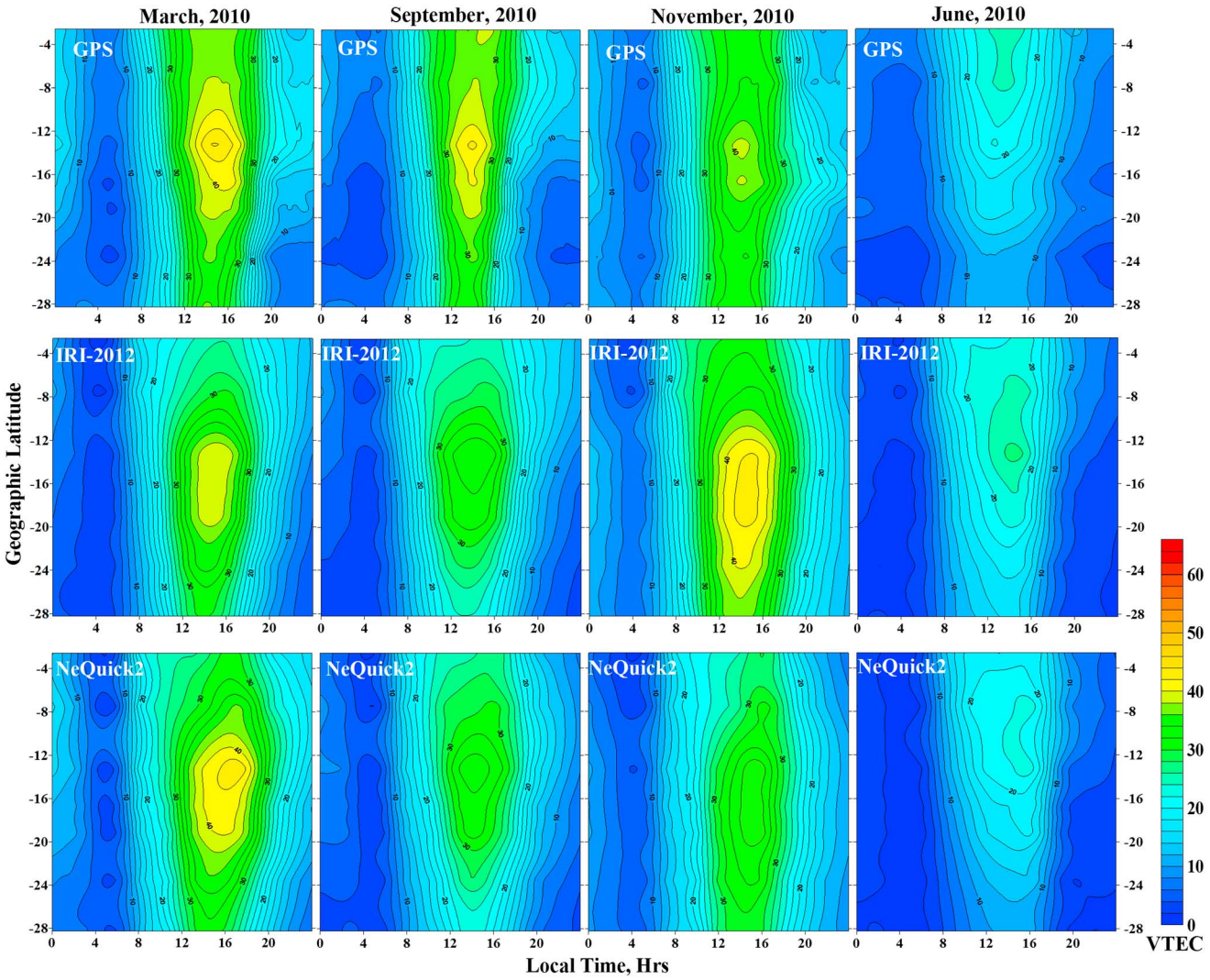

Figure 5. Contour plots showing the variation of TEC as a function of local time and geographic latitude from GPS (top row), IRI-2012 (middle row) and NeQuick2 (bottom row) during the months of March, September, November, and December 2010 representing vernal equinox, autumn equinox, summer, and winter seasons.

TEC values. This indicates that the IRI-2012 and NeQuick2 models underestimate the GPS TEC during increased solar activity conditions while they give better estimates of GPS TEC during the low solar activity conditions.

3.2. Equatorial Ionization Anomaly-Latitudinal Variation of TEC

The typical equatorial electrodynamical phenomena, namely, the equatorial ionization anomaly, is the major cause for the large variabilities and altitudinal as well as the latitudinal gradients in the electron density variations over the equatorial and low-latitude sectors. To understand the variations in the formation of the EIA during different seasons, and also to compare it with the model-derived EIA behavior, the monthly mean diurnal values of TEC from GPS, IRI-2012, and NeQuick2 have been derived at all the seven considered locations. In Figure 5 are presented the contour plots of the diurnal variation of TEC as a function of latitude during the months of March, September, November, and June 2010 representing the autumn equinox, vernal equinox, summer, and winter seasons, respectively. The top row represents the variations of TEC from GPS and the middle row represents the variations of TEC from the IRI-2012 model while the bottom row represents the variations of TEC from the NeQuick2 model. The GPS TEC shows a maximum of about 45 TECU at the anomaly crest during equinoctial months and around 35 TECU during summer and around 25 TECU during winter season. The maximum TEC at the anomaly crest derived from the IRI-2012 and NeQuick2 models varies between 35 and 45 TECU during equinoctial and summer

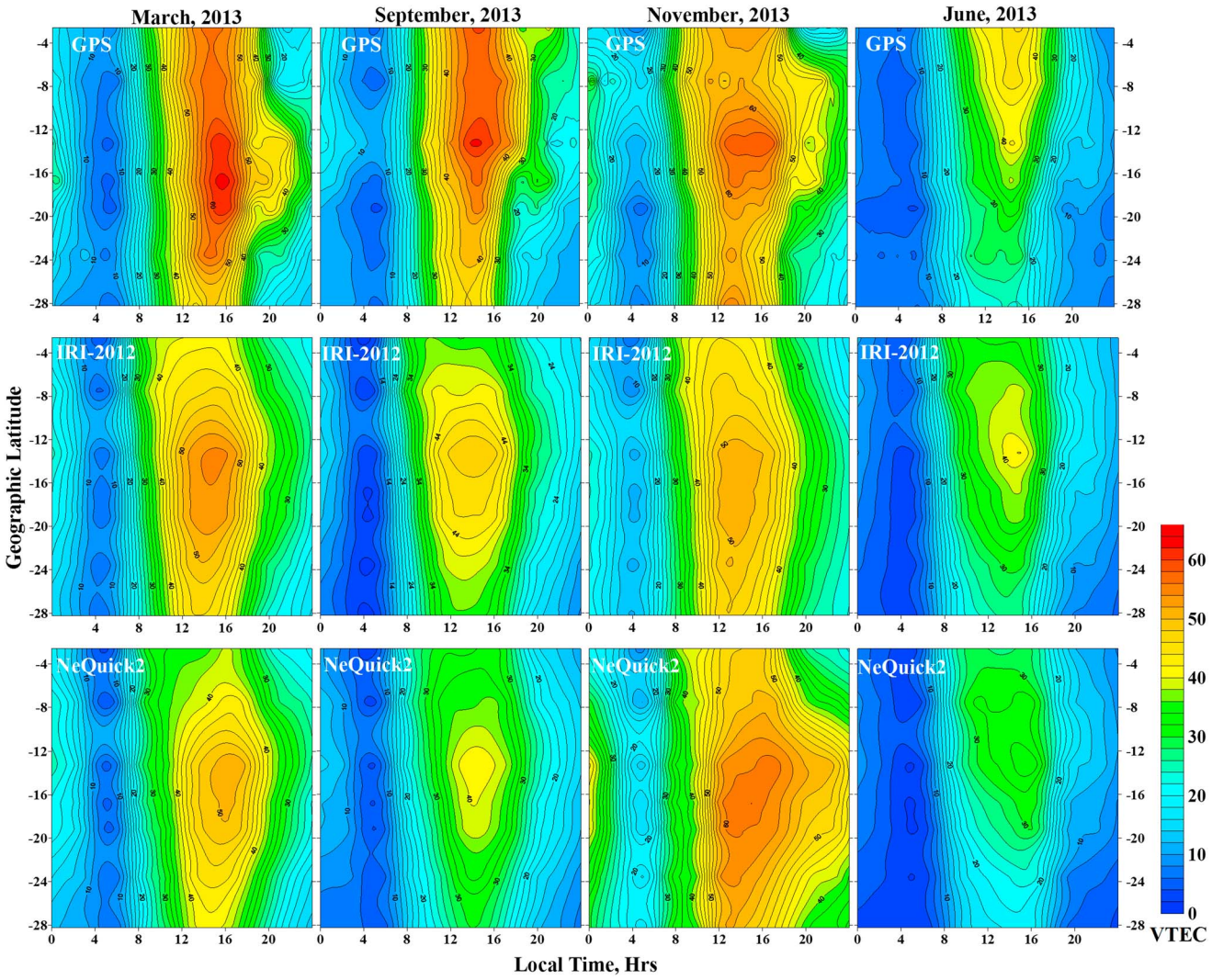

Figure 6. Contour plots showing the variation of TEC as a function of local time and geographic latitude from GPS (top row), IRI-2012 (middle row) and NeQuick2 (bottom row) during the months of March, September, November, and December 2013 representing vernal equinox, autumn equinox, summer, and winter seasons.

months while it is around 25 TECU during winter months. The GPS-measured TEC shows strong anomaly peak during equinoctial months, while the IRI-2012 shows the strong anomaly peak during summer and the NeQuick2 model shows strong peak during the autumn equinox. During the equinoctial and summer months, the EIA peak is observed between 12° and 15° geographic South latitudes in the GPS TEC observations, between 13° and 20° latitudes in the IRI-2012-modeled TEC values, and between 12° and 19° latitudes in the NeQuick2 model-derived TEC values. During the winter month of June 2010, it is observed from the GPS observations that the EIA is weak without forming the ionization anomaly crest while keeping most of the ionization over the equator. The TEC variations derived from the IRI-2012 and NeQuick2 models show the anomaly crest around 10° geographic latitude during the winter month of June 2010. In general, it observed that the strength and locations of the EIA crest from the two models are nearly comparable with the GPS observations during equinoctial and summer months whereas during winter months, both the models shows the formation of the weak EIA crest while the EIA crest is not seen in the GPS observations.

Similar analysis has been carried out using the TEC data from GPS and both the models during the year 2013 to study the behavior of the EIA crest in the increased solar activity conditions. In Figure 6 are presented the contour plots of the diurnal variations of TEC as a function of latitude during four different months representing four different seasons. The formation of the strong anomaly crest is observed during the

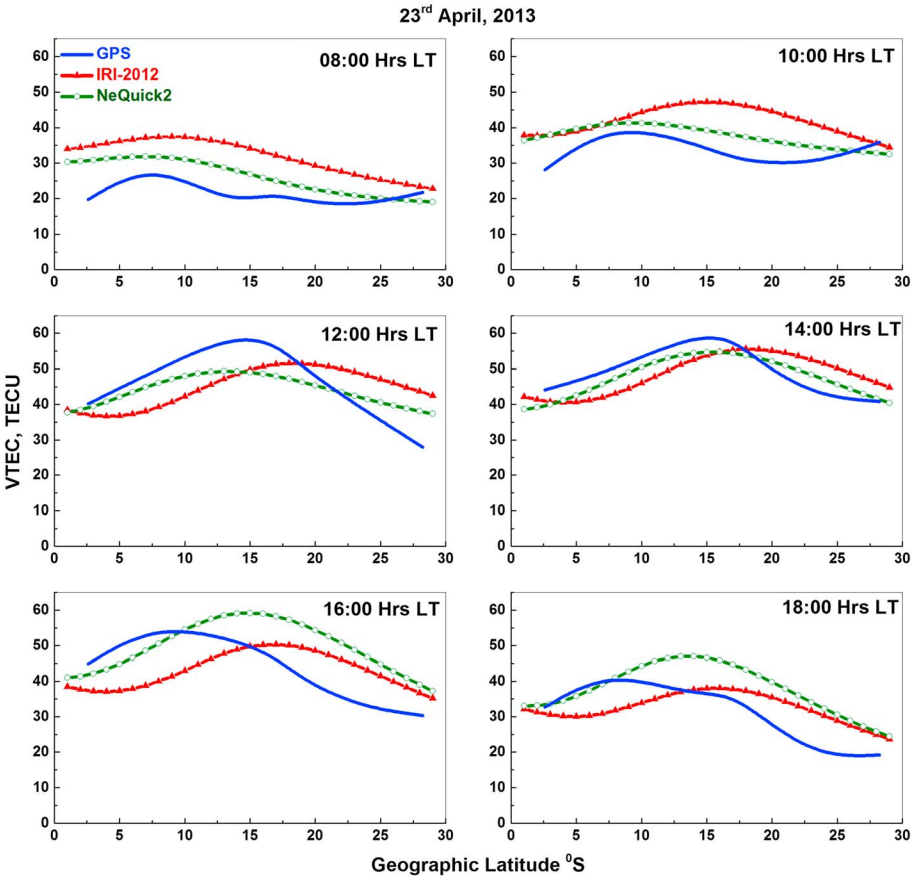

Figure 7. Typical examples of the latitudinal variation of TEC from GPS (blue curves), IRI-2012 (red curves with triangles), and NeQuick2 (green curves with circles) at different local times on 23 April 2013.

equinoctial and summer months in the experimental and the model-derived TEC variations. The GPS TEC shows a maximum of around 60 to 65 TECU at the EIA crest during equinoctial and summer months. The peak TEC at the EIA crest during the equinoctial and summer months varies around 50 TECU in the IRI-2012-modeled TEC values while it varies between 50 and 55 TECU in the NeQuick2 model-derived TEC values. It is clearly observed from these figures that the TEC at the EIA crest derived from both the models are much lower compared to that derived from GPS during equinoctial and summer months. Significant nighttime ionization is observed during postsunset hours at the anomaly crest locations during March and November 2013. The NeQuick2 model shows this nighttime ionization only during November 2013 while it is not observed in the IRI-2012 model-derived TEC variations. In the winter month of June 2013, the GPS TEC shows a very weak anomaly and most of the ionization is over the equator, whereas the IRI-2012 and NeQuick2 models shows the formation of the EIA around 13° geographic South. It is clearly observed from these observations that the IRI-2012 and NeQuick2 models shows significant differences in predicting the strength and the location of the EIA crest during the increased solar activity conditions. It is also observed from the latitudinal variation of GPS TEC that the ionization increases very rapidly in the prenoon hours at all the latitudes with pronounced latitudinal gradients at and around the anomaly crest locations in the presence of the well-developed EIA.

With a view to look into the variations in the equatorward and poleward ionization gradients, the latitudinal variation of TEC from GPS, IRI-2012, and NeQuick2 models for every 2 h interval from 0800 to 1800 h LT on a typical day of 23 April 2013 is presented in Figure 7. The blue-colored curves represent the variation of GPS TEC while the red-colored curves with triangles and green-colored curves with circles represent the variations of TEC from the IRI-2012 and NeQuick2 models, respectively. It is seen from this figure that at 0800 h LT, the GPS TEC shows an additional ionization of around 5 TECU between 5° and 10°

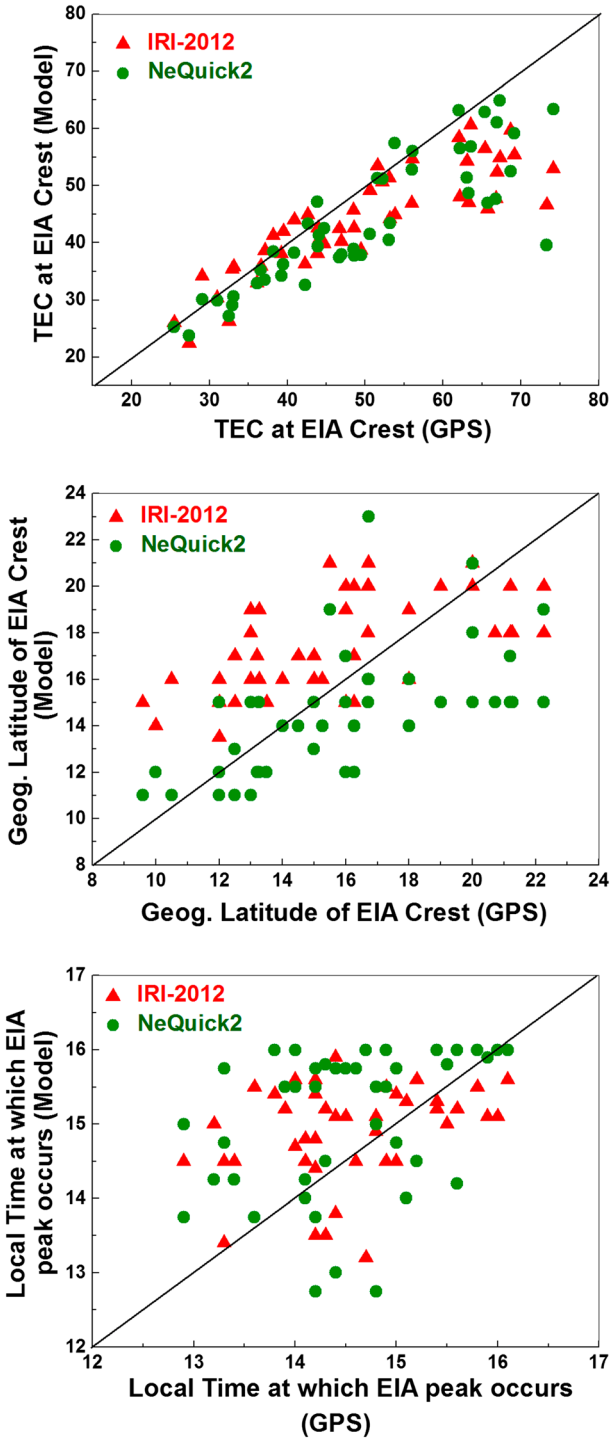

Figure 8. Scatterplots showing the variation of the TEC at the EIA crest, geographic latitude of EIA crest, and local time of the occurrence of the crest derived from GPS, IRI-2012, and Nequick2 models during a 4 year period from 2010 to 2013.

latitudes while the ionization is almost at the same level in the remaining latitudes. The NeQuick2 model shows 30 TECU from equator to around 8° latitude and decreases to 20 TECU at 30° latitude. The IRI-2012 also shows similar type of variation with 35 TECU from equator to 8° latitude which decreases to around 25 TECU at 30° latitudes. At 1000 h LT, the TEC increases by nearly 10 TECU at all the latitudes in the GPS and model-derived values. The GPS and NeQuick2 models show more ionization around 9° latitude whereas the IRI-2012 model shows more ionization around 15° latitude. At 1200 h LT (the EIA is supposed to develop), the GPS TEC shows a well-developed EIA with a peak of 57 TECU around 15° latitude. The IRI-2012 model shows the peak of 50 TECU around 18° latitude while the NeQuick2 models show a peak TEC of 48 TECU around 12° latitude. At 1400 h LT, the strong EIA in the GPS and IRI-2012 TEC persist with the peak TEC around 15° and 18° latitudes, respectively. The NeQuick2 model shows a peak of 52 TECU at 15° latitude. The strength of the EIA starts decreasing in GPS and IRI-2012 model-derived TEC values at 1600 h LT while the NeQuick2 model shows the strong EIA at this local time with a peak TEC of 57 TECU around 15° latitudes. By the evening hours of 1800 h LT the TEC variations from GPS as well as the IRI-2012 and NeQuick models show a decreases in the strength of the EIA with the TEC peak moving toward the equator. These observations reveal that the GPS TEC shows the formation of the well-developed EIA between 1200 and 1400 h LT with a peak TEC of 57 TECU around 15° latitude. The IRI-2012 model also shows the strong EIA around 1200 and 1400 h LT while overestimating the location of the crest (showing at 18° latitude) and underestimating the peak TEC (50 TECU) compared with those of the GPS TEC variations. On the other hand, the location and strength of the crest of the EIA from GPS TEC and NeQuick2 model are nearly comparable while the well-developed EIA occurs in a delayed time between 1400 and 1600 h LT in the NeQuick2-modeled TEC variations. Further, strong poleward gradients in TEC compared to the equatorward gradients are observed in the GPS TEC variations during 1200 and 1400 h LT.

Whereas the IRI-2012 and NeQuick2 models show similar gradients of TEC on either sides of the EIA crest and the gradients are less than those observed in the GPS TEC variations.

3.3. Comparison of the Strength, Location, and Local Times of the EIA Crest

The important parameters needed to characterize the EIA crest are the peak TEC, latitude of the occurrence of TEC peak, and the local time at which the well-developed EIA is seen. The TEC values derived from GPS, IRI-2012, and NeQuick2 models for every month during the 4 year period from 2010 to 2013 at all the considered locations are used to derive the above mentioned three typical parameters of the EIA crest. In Figure 8 are presented the scatterplots showing the variation of TEC at the EIA crest, geographic latitude of the EIA crest, and local time of the occurrence of the crest derived from GPS, IRI-2012, and NeQuick2 models during 2010 to 2013. The red-colored triangles represent the variation of IRI-2012 model-derived parameters versus GPS observations while the green-colored dots represents those of the NeQuick2 model versus GPS observations. It is seen from this figure that the TEC at the EIA crest varies from 25 to 70 TECU in the GPS measurements, while the models show the TEC at the EIA crest between 25 and 65 TECU. It is interesting to note that both model-derived TEC show good correlation with the GPS TEC when the peak ionization at the EIA crest is low (between 25 and 45 TECU). When the peak ionization at the EIA crest increases (above 45 TECU), both the models are underestimating the strength of the EIA crest. It is observed from the GPS TEC variations that the location of the EIA crest varies between 9° and 22° geographic latitudes. Further, the IRI-2012 model predictions reveal that the location of the EIA crest varies between 14° and 22° latitudes while the crest is observed between 11° and 20° latitudes in the NeQuick2 model predictions. It is also seen from this figure that the well-developed anomaly is found between 13 and 16 h LT in the GPS observations whereas the IRI-2012 and NeQuick2 models predicting the occurrence of the EIA peak in a delayed local time hour compared to those of the GPS observations in most of the cases.

4. Discussion

Since its initiation, the IRI model is being updated regularly by incorporating different data sets available over the globe and using better modeling techniques. Similarly, the NeQuick model has also been updated in the recent years to its next version, i.e., the NeQuick2 incorporating several modifications. Several comparative studies are being carried out to validate different versions of these models using the experimental data over different parts of the globe to bring out agreements and disagreements between the models and experiments, and many studies reveal that these models shows better performance over the midlatitudes and high latitudes compared to the equatorial and low latitudes [*McNamara*, 1984, 1985]. *Abdu et al.* [1996] compared the IRI-90 model predictions with the experimental measurements of TEC and *F* layer parameters such as the f_oF_2 and h_mF_2 in the equatorial and low latitudes of Brazilian and Asian sectors. They reported that the IRI shows good agreement in intermediate solar activity conditions and underestimates the anomaly region TEC during solar maximum. *Iyer et al.* [1996] and *Singh et al.* [1996] have also shown that the IRI-90 model overestimates the TEC during low solar activity and underestimates during high solar activity conditions at the anomaly crest locations in the Indian and east Asian longitude sectors. Later, it was reported that the NeQuick and IRI-01 corrected methods provide better agreement with the TEC observations [*Sethi et al.*, 2011; *Bhuyan and Borah*, 2007]. The limitations of IRI-2001 model were overcome in the next version (IRI-2007) by applying NeQuick topside option [*Radicella and Leitinger*, 2001; *Coisson et al.*, 2006]. *Prasad et al.* [2012] compared the GPS TEC measurements with IRI predictions in the Indian equatorial and low latitudes and reported that the IRI-2007 model (with NeQuick option for topside ionosphere) shows improved performance compared to those of IRI-2001 versions. *Jesus de et al.* [2011] have also reported that the variations of IRI-2007 simulations of f_oF_2 show better agreement with the observed values than IRI-2001 over low-latitude stations in the Brazilian sector. However, it was also reported that the IRI-2007 model shows significant deviations from the GPS measurements with more differences during equinoctial months at the anomaly crest locations [*Prasad et al.*, 2012; *Jesus de et al.*, 2011; *Kumar et al.*, 2014]. Further, it was reported that the IRI-2007 model with NeQuick option for topside ionosphere overestimates the GPS TEC during daytime and underestimates during nighttime hours at the equatorial and low latitudes [*Luhr and Xiong*, 2010; *Venkatesh et al.*, 2011; *Sethi et al.*, 2011; *Olwendo et al.*, 2013].

The present study carried out to validate the recently updated versions; the IRI-2012 and NeQuick2 models reveal that these latest updated models show improved performance during the low solar activity conditions. Both the models predicted the GPS TEC with improved accuracy during the low solar activity year with few

differences at and around the anomaly crest locations during equinoctial months. During the increased solar activity conditions, the discrepancies in the earlier versions are still retained in the updated versions where both the models are underestimating the GPS TEC during daytime hours and overestimating the GPS TEC during nighttime hours at all latitudes with large differences at and around the anomaly crest locations. Significant differences have also been observed in between the TEC values derived using the IRI-2012 and NeQuick2 models. The peak TEC value at the EIA crest is comparable with the GPS observations during the low solar activity years while the model underestimates the strength of the EIA crest during the increased solar activity conditions. *Nigussie et al.* [2013] have also compared the GPS TEC with the IRI-2007 and NeQuick2 model-derived TEC and reported good agreement during December solstice and more discrepancies during other seasons in the African equatorial sector. Comparative study between the GPS TEC and models at a near equatorial station, Banting in the East Asian sector also revealed the improved performance of IRI-2012 model compared to the earlier IRI-2007 version while reporting more discrepancies between the modeled and experimental TEC during equinoctial months [*Leong et al*., 2014].

The prediction of TEC using IRI-2012 and NeQuick2 is mainly associated with the proper estimation of the *F* layer peak electron density as well as the ionospheric thickness and electron density profile shape parameters (such as the slab-thickness, scale height, bottomside thickness parameter (B_0) and bottomside shape parameter (B_1)) at different altitudes. Therefore, the differences in the model-derived TEC can be due to the discrepancies in estimating the peak density or the thickness parameter or due to both inadequately modeled peak density and thickness parameters. The variations of topside scale height from the IRI-2007 model with NeQuick option were compared with the topside scale heights derived using ionosonde and Republic Of China SATellite (ROCSAT) measurements over the Indian low-latitude sector by *Venkatesh et al.* [2011] and it was reported that the IRI-derived scale height is lower during daytime hours and higher during nighttime hours compared to those of the measured values. This could make the electron density profile skewer during daytime hours and flat during nighttime hours leading to the underestimation and overestimation of TEC during day and nighttime hours, respectively. *Rios et al.* [2007] have compared the IRI-modeled slab-thickness with the experimental data and reported that the model-derived slab-thickness is lower during daytime hours and higher during nighttime hours compared to those of the experimental slab-thickness values. The present study also revealed several differences between the modeled and experimental TEC and also there are significant differences between the IRI-2012 and NeQuick2 model-derived TEC values.

To understand the causes for the observed discrepancies, the ionosonde data over a typical anomaly crest location, Sao Jose dos Campos, are considered to derive the bottomside vertical electron density profiles using POLAN true height inversion algorithm. These bottomside electron density profiles are compared with the IRI-2012 and NeQuick2 model-derived electron density profiles during different solar activity conditions. The vertical electron density profiles derived from the ionosonde and both the models at each 1 h interval on a typical day of 19 October 2010 are presented in Figure 9. The blue-colored profiles are the ionosonde-derived profiles, the red-colored profiles with triangles are those derived from the IRI-2012 model, and the green-colored profiles with circles are from the NeQuick2 model. It is seen from this figure that both the models overestimate the *F* layer peak in several cases particularly during the nighttime hours while the bottomside profiles are comparable in some of the cases. The monthly mean variations of TEC during a low solar activity year (Figure 2) shows that at and around the anomaly crest locations, the TEC values from both the models are higher than the GPS TEC in the afternoon and nighttime hours. The electron density profiles presented in Figure 9 for a typical anomaly crest locations also reveal that both the models overestimate the *F* layer peak density in the afternoon and nighttime hours. Further, it is observed from the monthly mean TEC values (Figure 2) that at and around the anomaly crest locations, the IRI-2012-derived TEC is more than that of NeQuick2 model between 0900 and 1300 h LT while the GPS-derived TEC lies in between the IRI-2012- and NeQuick2-modeled TEC values. The electron density profiles in Figure 9 shows that at and around the anomaly crest locations, the IRI-2012 model-derived peak density is higher than that of NeQuick2 model while both these models are underestimating the ionosonde-derived peak density.

Similarly, the vertical electron density profiles over an anomaly crest location during a typical day of 19 October 2013 representing the high solar activity conditions are presented in Figure 10. It is observed from this figure that in many cases, the *F* layer peak densities from the models show significant differences compared to those of the ionosonde measurements while the bottomside profiles are comparable with the ionosonde profiles in few cases during nighttime hours. The monthly mean TEC variations during the

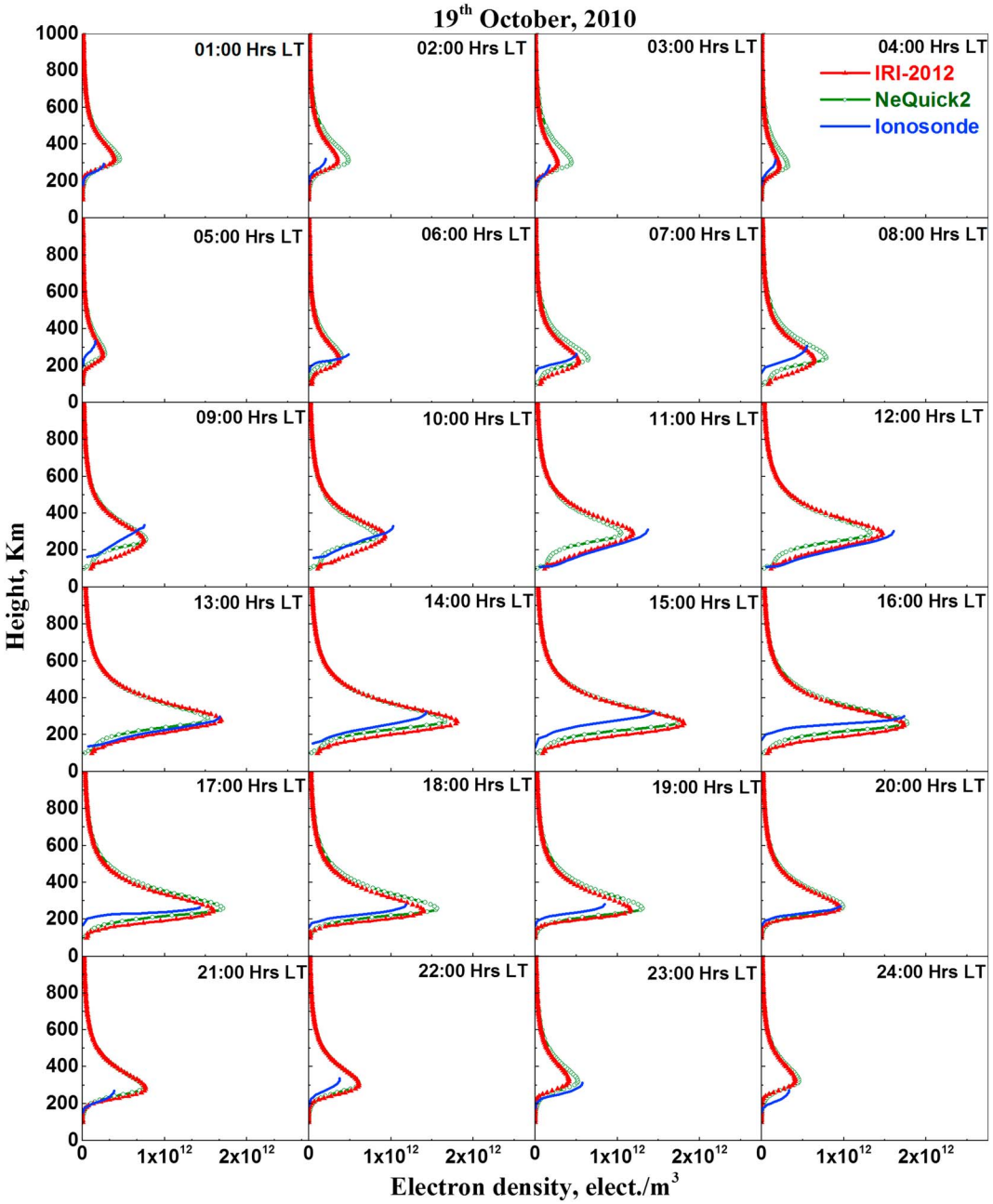

Figure 9. Vertical electron density profiles derived from ionosonde (blue colored), IRI-2012 model (red-colored curves with triangles), and NeQuick2 models (green-colored curves with circles) during different time intervals on 19 October 2010.

increased solar activity conditions presented in Figure 3 reveal that at and around the anomaly crest locations, the models show better performance only between 0500 and 1300 h LT during the equinoctial and summer months. The electron density profiles in Figure 10 show that the models overestimate the ionosonde-derived *F* layer peak density between 0500 and 0900 h LT and show comparable peak density values between 1000 and 1300 h LT with significant differences in the shape and heights of the profiles between the model and experiments during all these hours. Further, the mean TEC variations presented in Figure 3 shows that at and around anomaly crest locations, the TEC values from IRI-2012 and NeQuick2 are comparable between 0500 and 1300 h LT while the IRI-derived TEC is less than that of NeQuick2 during all other time intervals of the day. The IRI-2012 and NeQuick2 model-derived profiles in Figure 10 also reveal that the shapes of the IRI-2012- and NeQuick2-modeled topside profiles and the peak densities

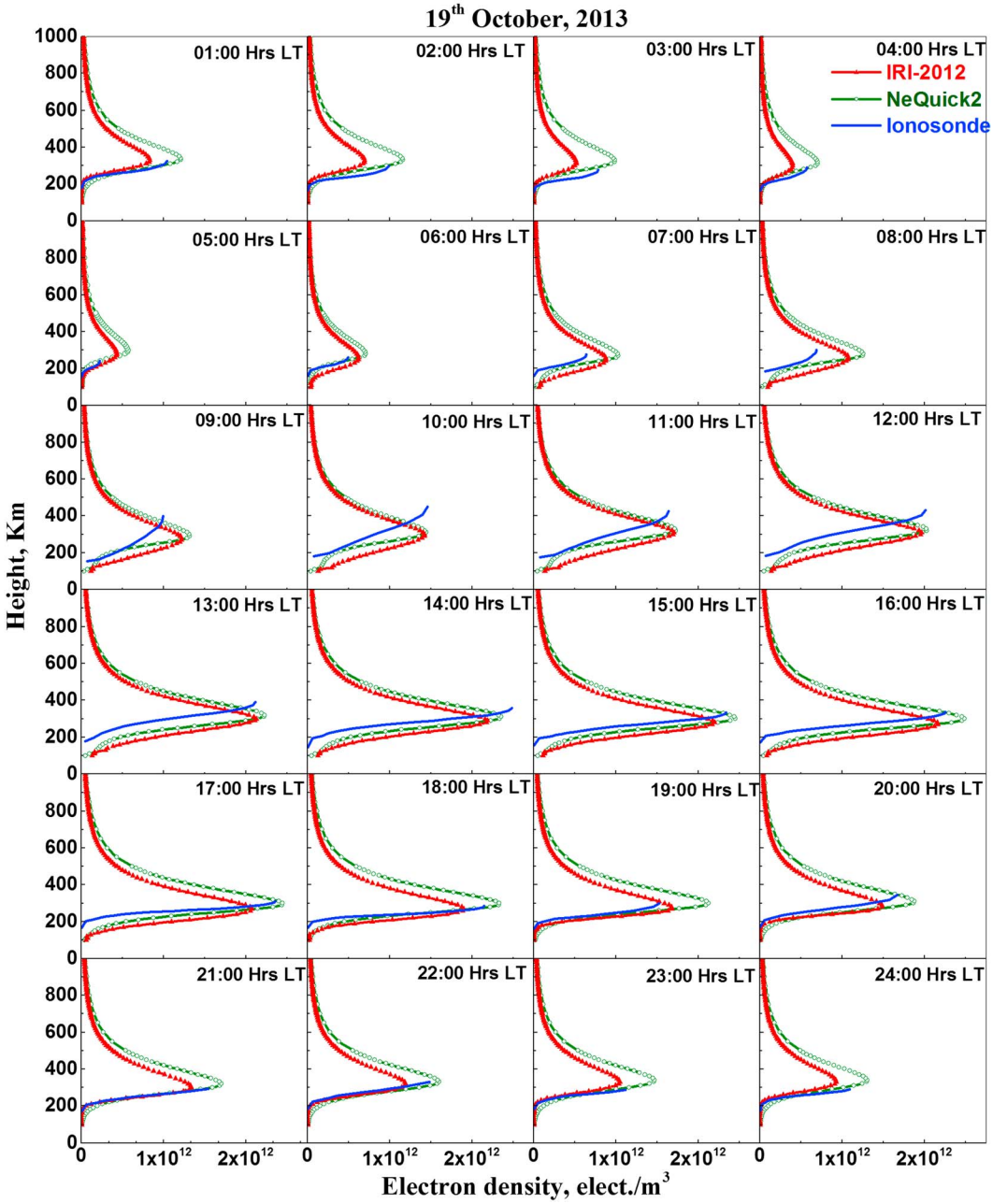

Figure 10. Vertical electron density profiles derived from ionosonde (blue colored), IRI-2012 model (red-colored curves with triangles), and NeQuick2 models (green-colored curves with circles) during different time intervals on 19 October 2013.

are comparable between 0500 and 1300 h LT while the IRI-2012 model underestimates the peak density during the all the remaining hours of the day.

Further, the vertical electron density profiles derived from ionosonde, IRI-2012, and NeQuick2 model during the above two typical days are used to derive the diurnal variations of the bottomside thickness (B_0) and shape (B_1) parameters over the anomaly crest location SJSC and the results are presented in Figure 11. It is seen from this figure that the diurnal variation of B_0 shows higher values during daytime hours and lower values during nighttime hours with the day maximum around noontime hours. The models derived B_0 also show similar type of diurnal behavior while the day maximum is at the lower level in the NeQuick2 model-derived B_0 variations. The ionosonde-derived B_0 shows a day maximum of about 170 km

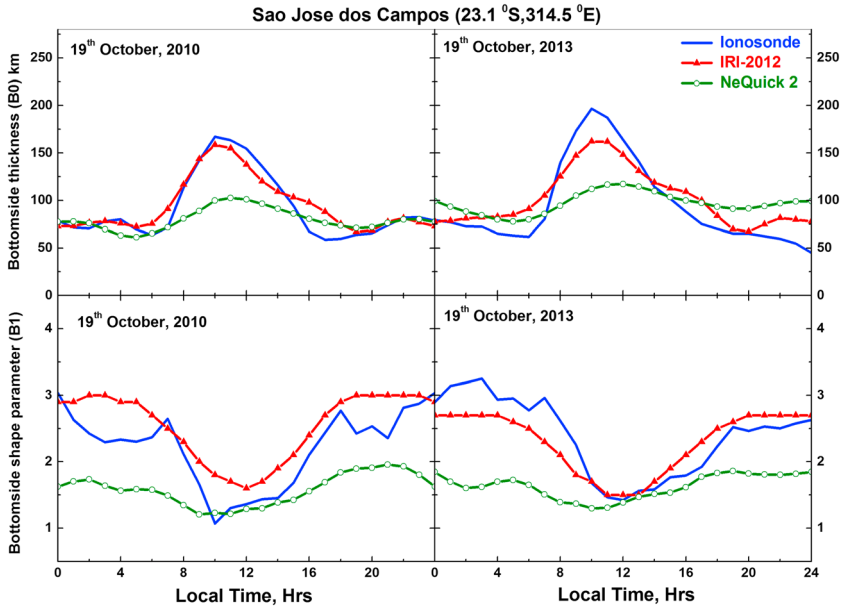

Figure 11. The diurnal variations of bottomside thickness (B_0) and shape (B_1) parameters derived from ionosonde, IRI-2012, and NeQuick2 models over the anomaly crest location, Sao Jose dos Campos, on two typical days of low and increased solar activity years.

during low solar activity while it is around 200 km during increased solar activity. The IRI-2012-derived B_0 shows the day maximum around 150 km during both solar activity conditions. The NeQuick2 model-derived B_0 shows an increase of about 20 km during all hours on a high solar activity day compared to that on a low solar activity day. In general, the IRI-2012 shows good predictions of ionosonde measurements during the low solar activity with significant differences during the increased solar activity. The NeQuick2-derived B_0 values are comparable with those of the ionosonde during the nighttime hours of the low solar activity. The diurnal variation of B_1 shows lower values during daytime hours compared to those during nighttime hours. The IRI-2012 also shows similar type of diurnal behavior while this is not more pronounced in the NeQuick2 model predictions. The ionosonde-derived B_1 varies between 1 and 3 with the day minimum around noontime hours. The IRI-2012 model overestimates the ionosonde-derived B1 values during the low solar activity and in the afternoon hours of the increased solar activity. The NeQuick2 model-derived B_1 varies from 1.3 to 1.8 and always underestimating those of the ionosonde measurements except during few cases in the noontime hours.

It is observed from a comparison of the vertical electron density profiles that during 01:00 to 05:00 h LT, the IRI-2012 reproduces better estimates of ionosonde measurements during the low solar activity period (Figure 9) while the NeQuick2 model produces better results during the increased solar activity conditions (Figure 10). However, as it is seen in Figure 11, during both days from 00:00 to 07:00 h LT and 17:00 to 24:00 h LT, the IRI-2012 model shows better estimates of profile shape parameter compared to that of the NeQuick2 model. In the IRI-2012 model, the URSI option is used for the estimation of *F* layer peak parameters, and the thickness and shape parameters are determined using ABT-2009 option. Whereas the NeQuick2 model uses International Radio Consultative Committee coefficients for the estimation of *F* layer peak parameters. Hence, the differences observed in the two models in the estimation of electron density and profile parameters could be because of different methods used in the models.

The present observations indicate that the differences in the TEC values in between the two models coincide with the discrepancies in the estimation of *F* layer peak density values with the simultaneous differences in the bottomside profile parameters. The comparison of models derived outputs with those of the experimental values shows that the differences in TEC can be due to the discrepancies of the models in estimating the peak density as well as the shape and thickness parameters of the electron density profiles. The discrepancies between the measured and model-derived profile parameters have also been reported using the earlier versions of the IRI model over equatorial and low-latitude sectors [*Sethi and Mahajan*, 2002; *Lei et al.*, 2004;

Blanch et al., 2007; *Zhang et al*., 2008]. Further, it is known that the topside ionosphere contributes more to the TEC value compared to that of the bottomside contribution. Hence, along with the differences in the *F* layer peak density, height, and bottomside profile parameters, the discrepancies in the topside scale height (which is the most important parameter in deriving the topside profile) can contribute significantly for the inaccuracy in the estimation of TEC values. Using the Constellation Observing System for Meteorology, Ionosphere and Climate (COSMIC) radio occultation measurements, *Potula et al.* [2011] reported that the IRI model-derived scale height values over the equatorial and low latitudes differ significantly with the experimental scale height values. Using ROCSAT satellite in situ measurements, *Tulasi Ram et al.* [2009] and *Venkatesh et al.* [2011] have also reported significant differences in the shapes of the topside electron density profiles and corresponding scale height values in the IRI-2007 (with NeQuick option for topside ionosphere) predictions over equatorial and low latitudes. Using the GPS and ionosonde measurements in the African equatorial and low-latitude sectors, *Nigussie et al.* [2013] have also attributed the discrepancies between the GPS-measured and IRI and NeQuick2 model-derived TEC to the inadequately modeled slab-thickness parameters.

There are two major sources for the variabilities in the electron density over equatorial and low latitudes. One is the changes in the solar ionizing radiation causing corresponding variations in the production and loss rates leading to the electron density variations. Second, the large spatiotemporal variabilities in the electron density are due to the dynamical phenomena namely the EIA which is a consequence of the equatorial fountain effect. The driving force behind this fountain effect is the $\mathbf{E} \times \mathbf{B}$ drifts over the equator being controlled by the strength of the Equatorial Electrojet (EEJ). The EEJ shows significant variations with local time, season, and solar activity leading to the corresponding variabilities in the electron density distribution over equatorial and low latitudes. It has also been reported that the diurnal variation of topside effective scale height does not closely follow the diurnal variation pattern of the plasma scale height and/or plasma temperature and is largely controlled by the vertical $\mathbf{E} \times \mathbf{B}$ drifts due to the zonal electric fields at equatorial latitudes [*Tulasi Ram et al.*, 2009]. Thus, quantifying the effect of the EEJ and $\mathbf{E} \times \mathbf{B}$ drifts on the strength of the EIA and on the variabilities of the electron density distribution could be very much useful for achieving more accuracy in the model predictions over the equatorial and low latitudes.

5. Summary

The simultaneous measurements of GPS TEC at seven different identified locations along a common longitude of 315°E in the Brazilian sector during a 4 year period from 2010 to 2013 in the increasing phase of the solar activity are used to validate the latest available IRI-2012 and NeQuick2 models. It is observed that both the models predicted the GPS TEC with improved accuracy during the low solar activity year with few differences during daytime hours. During the increased solar activity conditions, the discrepancies in the earlier versions of the models are still retained in the updated versions where both the models underestimate the GPS TEC during daytime hours and overestimated the GPS TEC during nighttime hours at all latitudes with large differences at and around the anomaly crest locations. At and around the anomaly crest locations, the increased ionization in the nighttime hours observed in GPS TEC variations (particularly during the increased solar activity conditions) are not well pronounced in the IRI-2012-derived TEC variations while they are marginally observed in the NeQuick2-modeled TEC values. Comparing the performance of the IRI-2012 and NeQuick2 models, the IRI model overestimates the NeQuick2 model-derived TEC and the GPS TEC in the morning hours (between 0500 and 1300 h LT) of vernal equinox and summer months during the low solar activity years. On the contrary, during the equinoctial and winter months of increased solar activity conditions, the IRI-2012- and NeQuick2-modeled TEC values are comparable with each other between 0500 and 1300 h LT and the IRI-2012-derived TEC is less than the NeQuick2-derived TEC during all the remaining hours of the day. The strength of the anomaly crest (peak TEC at the EIA crest) is well represented by both the models during the low solar activity years while during the increased solar activity years, both the models are underestimating the strength of the EIA crest. During southern winter months, the GPS observations do not show the formation of the EIA and most of the ionization is observed over the equator. Whereas both the IRI-2012 and NeQuick2 models show the presence of the weak EIA during the winter months with peak TEC observed around 10° latitudes. However, it is interesting to note that both the models predicted the peak TEC at the EIA crest with reasonable accuracy in more than half of the cases, and in the remaining cases (with higher ambient ionization), the models underestimated the peak TEC at the EIA crest and these cases could be corresponding to the increased solar activity conditions. Further, it is generally observed that the

IRI-2012 model is overestimating the location of the EIA crest while the NeQuick model is underestimating the location of the EIA crest. The strong poleward gradients compared to the equatorward gradients observed in the GPS TEC variations are not seen either in the IRI-2012 or NeQuick2 model-derived TEC values. An insight into the variations of the vertical electron density profiles and related profile parameters reveal that the differences in between the TEC values derived from both the models coincide well with the discrepancies in the estimation of *F* layer peak density with simultaneous differences in profile parameters. Further, the differences between the model-derived and GPS-measured TEC (particularly during increased solar activity conditions) can be due to the discrepancies of the models in estimating both the peak density as well as the thickness and shape parameters of the electron density profiles.

Acknowledgments

One of the authors K.V. wishes to express his sincere thanks to the Fundação de Amparo a Pesquisa do Estado de Sao Paulo (FAPESP), Sao Paulo, Brazil, for providing financial support through the process 2012/08445-9 and 2013/17380-0. Authors wish to express their sincere thanks to IBGE (http://www.ibge.gov.br/home/geociencias/geodesia/rbmc/rbmc_est.php) for providing GPS TEC data used in this paper. Authors wish to express their sincere thanks to GSFC, NASA for providing online version of the IRI-2012 model (http://omniweb.gsfc.nasa.gov/vitmo/iri2012_vitmo.html). Authors also express their sincere thanks to the Telecommunications for Development (T/ICT4D) Laboratory of the Abdus Salam International Centre for Theoretical Physics, Trieste, Italy, for providing the NeQuick2 model (http://t-ict4d.ictp.it/nequick2/nequick-2-web-model).

Alan Rodger thanks the reviewers for their assistance in evaluating this paper.

References

Abdu, M. A., I. S. Batista, and J. R. deSouza (1996), An overview of IRI-observational data comparison in American (Brazilian) sector low latitude ionosphere, *Adv. Space Res.*, *18*(6), 13–22, doi:10.1016/0273-1177(95)00893-4.

Afraimovich, E. L., A. T. Altynetsev, E. A. Kosogorov, N. S. Larina, and L. A. Leonovich (2001), Ionospheric effects of the solar flares of September 23, 1998 and July 29, 1999 as deduced from global GPS network data, *J. Atmos. Sol. Terr. Phys.*, *63*(17), 1841–1849, doi:10.1016/S1364-6826(01)00060-8.

Appleton, E. V. (1946), Two anomalies in the ionosphere, *Nature*, *157*, 691–693.

Bagiya Mala, S., H. P. Joshi, K. N. Iyer, M. Aggarwal, S. Ravindrayan, and B. M. Pathan (2009), TEC variations during low solar activity period (2005–2007) near the equatorial ionospheric anomaly crest region in India, *Ann. Geophys.*, *27*, 1047–1057, doi:10.5194/angeo-27-1047-2009.

Batista, I. S., J. R. de Souza, M. A. Abdu, and E. R. de Paula (1994), Total electron content at low latitudes and its comparison with IRI90, *Adv. Space Res.*, *14*(12), 87–90, doi:10.1016/0273-1177(94)90246-1.

Bhuyan, P. K., and R. R. Borah (2007), TEC derived from GPS network in India and comparison with IRI, *Adv. Space Res.*, *39*(5), 830–840, doi:10.1016/j.asr.2006.12.042.

Bidaine, B., and R. Warnant (2010), Assessment of the NeQuick model at mid-latitudes using GNSS TEC and ionosonde data, *Adv. Space Res.*, *45*(9), 1122–1128, doi:10.1016/j.asr.2009.10.010.

Bilitza, D. (1986), International reference ionosphere: Recent developments, *Radio Sci.*, *21*, 343–346, doi:10.1029/RS021i003p00343.

Bilitza, D. (Ed.) (1990), International Reference Ionosphere 1990, *NSSDC Report 90-22*, Greenbelt, Md.

Bilitza, D. (2001), International Reference Ionosphere 2000, *Radio Sci.*, *36*, 261–275, doi:10.1029/2000RS002432.

Bilitza, D., and B. W. Reinisch (2008), International Reference Ionosphere 2007: Improvements and new parameters, *Adv. Space Res.*, *42*(4), 599–609, doi:10.1016/j.asr.2007.07.048.

Bilitza, D., M. Hernández-Pajares, J. M. Juan, and J. Sanz (1998), Comparison between IRI and GPS-IGS derived electron content during 1991–97, *Phys. Chem. Earth*, *24*(4), 311–319.

Bilitza, D., D. Altadill, Y. Zhang, C. Mertens, V. Truhlik, P. Richards, L. A. McKinnell, and B. Reinisch (2014), The International Reference Ionosphere 2012: A model of international collaboration, *J. Space Weather Space Clim.*, *4*, A07, doi:10.1051/swsc/2014004.

Blanch, E., D. Arrazola, D. Altadill, D. Buresova, and M. Mosert (2007), Improvement of IRI B0, B1 and D1 at mid-latitudes using MARP, *Adv. Space Res.*, *39*(5), 701–710, doi:10.1016/j.asr.2006.08.007.

Brunini, C., M. A. Van Zele, A. Meza, and M. Gende (2003), Quiet and perturbed ionospheric representation according to the electron content from GPS signals, *J. Geophys. Res. 108*(A2), 1056, doi:10.1029/2002JA009346.

Coisson, P., S. M. Radicella, R. Leitinger, and B. Nava (2006), Topside electron density in IRI and NeQuick: Features and limitations, *Adv. Space Res.*, *37*(5), 937–942, doi:10.1016/j.asr.2005.09.015.

Davies, K., and G. K. Hartman (1997), Studying the ionosphere with global positioning system, *Radio Sci.*, *32*, 1695–1703, doi:10.1029/97RS00451.

Goodwin, G. L., J. H. Silby, K. J. W. Lynn, A. M. Breed, and E. A. Essex (1995), GPS satellite measurements: Ionospheric slab thickness and total electron content, *J. Atmos. Sol. Terr. Phys.*, *57*(14), 1723–1732, doi:10.1016/0021-9169(95)00093-H.

Hocke, K., and A. G. Pavelyev (2001), General aspect of GPS data use for atmospheric science, *Adv. Space Res.*, *27*, 1313–1320, doi:10.1016/S0273-1177(01)00141-7.

International Telecommunication Union (2003), Ionospheric propagation data and prediction methods required for the design of satellite services and systems, Recommendation, Geneva, pp. 531–7.

Iyer, K. N., H. P. Joshi, R. D. Jivarajani, and P. Arvindakshan (1996), Comparative study of TEC near the crest of the equatorial anomaly with IRI model for solar minimum to solar maximum, *Adv. Space Res.*, *18*(6), 233–236, doi:10.1016/0273-1177(95)00929-9.

Jee, G., R. W. Schunk, and L. Scherliess (2005), On the sensitivity of total electron content (TEC) to upper atmospheric/ionospheric parameters, *J. Atmos. Sol. Terr. Phys.*, *67*(11), 1040–1052, doi:10.1016/j.jastp.2005.04.001.

Jesus de, R., Y. Sahai, F. L. Guarnieri, P. R. Fagundes, A. J. de Abreu, V. G. Pillat, and W. L. C. Lima (2011), F-region ionospheric parameters observed in the equatorial and low latitude regions during medium solar activity in the Brazilian sector and comparison with the IRI-2007 model results, *Adv. Space Res.*, *47*(4), 718–728, doi:10.1016/j.asr.2010.10.020.

Jodogne, J. C., H. Nebdi, and R. Warnant (2004), GPS and ITEC from digisonde data compared with NeQuick model, *Adv. Radio Sci.*, *2*, 269–273, doi:10.5194/ars-2-269-2004.

Klobuchar, J. A. (1996), Ionospheric effects on GPS, in *Global Positioning System: Theory and Applications*, vol. 1, edited by B. W. Parkinson and J. J. Spilker, Progress in Astronautics and Aeronautics, 164, p. 485, American Inst. of Aeronautics and Astronautics, Reston, Va., doi:10.2514/5.9781600866388.0485.0515.

Kumar, S., A. K. Singh, and J. Lee (2014), Equatorial Ionospheric Anomaly (EIA) and comparison with IRI model during descending phase of solar activity (2005–2009), *Adv. Space Res.*, *53*(5), 724–733, doi:10.1016/j.asr.2013.12.019.

Langley, R., M. Fedrizzi, E. Paula, M. Santos, and A. Komjathy (2002), Mapping the low latitude ionosphere with GPS, *GPS World*, *13*(2), 41–46.

Lanyi, G. E., and T. Roth (1988), A comparison of mapped and measured total ionospheric electron content using global positioning system as beacon satellite observations, *Radio Sci.*, *23*(4), 483–492, doi:10.1029/RS023i004p00483.

Lei, J., L. Liu, W. Wan, S. R. Zhang, and J. M. Holt (2004), A statistical study of ionospheric profile parameters derived from Millstone Hill incoherent scatter radar measurements, *Geophys. Res. Lett.*, *31*, L14804, doi:10.1029/2004GL020578.

Leong, S. K., T. A. Musa, K. Omar, M. D. Subari, N. B. Pathy, and M. F. Asillam (2014), Assessment of ionosphere models at Banting: Performance of IRI-2007, IRI-2012 and NeQuick2 models during the ascending phase of Solar Cycle 24, *Adv. Space Res.*, doi:10.1016/j.asr.2014.01.026.

Luhr, H., and C. Xiong (2010), IRI-2007 model overestimates electron density during the 23/24 solar minimum, *Geophys. Res. Lett.*, *37*, L23101, doi:10.1029/2010GL045430.

Mannucci, A. J., B. D. Wilson, and C. D. Edwards (1993), A new method for monitoring the Earth's ionospheric total electron content using the GPS global network, *Proc. of ION GPS-93*, pp. 1323–1332, Inst. of Navigation, Salt Lake City, Utah.

Mannucci, A. J., B. D. Wilson, D. N. Yuan, C. M. Ho, U. J. Lindqwister, and T. F. Runge (1998), A global mapping technique for GPS derived ionospheric total electron content measurements, *Radio Sci.*, *33*, 565–582, doi:10.1029/97RS02707.

McNamara, L. F. (1984), Prediction of the total electron content using the international reference ionosphere, *Adv. Space Res.*, *4*(1), 25–50, doi:10.1016/0273-1177(84)90470-8.

McNamara, L. F. (1985), The use of the total electron content measurements to validate empirical models of the ionosphere, *Adv. Space Res.*, *5*(7), 81–90, doi:10.1016/0273-1177(85)90361-8.

Nava, B., P. Coïsson, and S. M. Radicella (2008), A new version of the NeQuick ionosphere electron density model, *J. Atmos. Sol. Terr. Phys.*, *70*(15), 1856–1862, doi:10.1016/j.jastp.2008.01.015.

Nigussie, M., S. M. Radicella, B. Damitie, B. Nava, E. Yizengaw, and K. Groves (2013), Validation of the NeQuick 2 and IRI-2007 models in East-African equatorial region, *J. Atmos. Sol. Terr. Phys.*, *102*, 26–33, doi:10.1016/j.jastp.2013.04.016.

Olwendo, O. J., P. Baki, P. J. Cilliers, C. Mito, and P. Doherty (2013), Comparison of GPS-TEC variations with IRI-2007 TEC prediction at equatorial latitudes during a low solar activity (2009–2011) phase over the Kenyan region, *Adv. Space Res.*, *52*, 1770–1779, doi:10.1016/j.asr.2012.08.001.

Potula, B. S., Y.-H. Chu, G. Uma, H.-P. Hsia, and K.-H. Wu (2011), A global comparative study on the ionospheric measurements between COSMIC radio occultation technique and IRI model, *J. Geophys. Res.*, *116*, A02310, doi:10.1029/2010JA015814.

Prasad, S. N. V. S., P. V. S. Rama Rao, D. S. V. V. D. Prasad, K. Venkatesh, and K. Niranjan (2012), On the variabilities of the Total Electron Content (TEC) over the Indian low latitude sector, *Adv. Space Res.*, *49*, 898–913, doi:10.1016/j.asr.2011.12.020.

Radicella, S. M., and R. Leitinger (2001), The evolution of the DGR approach to model electron density profiles, *Adv. Space Res.*, *27*(1), 35–40, doi:10.1016/S0273-1177(00)00138-1.

Rama Rao, P. V. S., S. Gopi Krishna, K. Niranjan, and D. S. V. V. D. Prasad (2006), Temporal and spatial variation in TEC using simultaneous measurements from the Indian GPS network of receivers during the low solar activity period of 2004–2005, *Ann. Geophys.*, *24*, 3279–3292, doi:10.5194/angeo-24-3279-2006.

Rawer, K. (1982), Replacement of the present sub-peak plasma density profile by a unique expression, *Adv. Space Res.*, *2*(10), 183–190, doi:10.1016/0273-1177(82)90387-8.

Rawer, K., D. Bilitza, and S. Ramakrishnan (1978), International Reference Ionosphere 78, *Special Report*, International Union of Radio Science (URSI), Brussels, Belgium.

Rios, V. H., C. F. Medina, and P. Alvarez (2007), Comparison between IRI predictions and digisonde measurements at Tucumán, *J. Atmos. Sol. Terr. Phys.*, *69*, 569–577, doi:10.1016/j.jastp.2006.10.004.

Seemala, G. K., and C. E. Valladares (2011), Statistics of total electron content depletions observed over the South American continent for the year 2008, *Radio Sci.*, *46*, RS5019, doi:10.1029/2011RS004722.

Sethi, N. K., and K. K. Mahajan (2002), The bottom side parameters B0, B1 obtained from incoherent scatter measurements during a solar maximum and their comparisons with the IRI-2001 model, *Ann. Geophys.*, *20*, 817–822, doi:10.5194/angeo-20-817-2002.

Sethi, N. K., R. S. Dabas, and S. K. Sarkar (2011), Validation of IRI-2007 against TEC observations during low solar activity over Indian sector, *J. Atmos. Sol. Terr. Phys.*, *73*, 751–759, doi:10.1016/j.jastp.2011.02.011.

Singh, L., J. K. Gupta, and T. R. Tyagi (1996), Comparison of Faraday rotation observations at Delhi with IRI model, *Adv. Space Res.*, *18*(6), 241–244, doi:10.1016/0273-1177(95)00931-0.

Titheridge, J. (1985), Ionogram analysis with the generalized program POLAN, *World Data Center Report*, UAG-93, WDC-A-STP, Boulder, Colo., pp. 194.

Tulasi Ram, S., S. Y. Su, C. H. Liu, B. W. Reinisch, and L. A. McKinnell (2009), Topside ionospheric effective scale heights (HT) derived with ROCSAT-1 and ground-based ionosonde observations at equatorial and midlatitude stations, *J. Geophys. Res.*, *114*, A10309, doi:10.1029/2009JA014485.

Valladares, C. E., J. Villalobos, M. A. Hei, R. Sheehan, S. Basu, E. MacKenzie, P. H. Doherty, and V. H. Rios (2009), Simultaneous observation of travelling ionospheric disturbances in the Northern and Southern Hemispheres, *Ann. Geophys.*, *27*, 1501–1508, doi:10.5194/angeo-27-1501-2009.

Venkatesh, K., P. V. S. Rama Rao, P. L. Saranya, D. S. V. V. D. Prasad, and K. Niranjan (2011), Vertical electron density and topside effective scale height (H_T) variations over the Indian equatorial and low latitude stations, *Ann. Geophys.*, *29*, 1861–1872, doi:10.5194/angeo-29-1861-2011.

Zhang, M. L., W. Wan, L. Liu, and J. K. Shi (2008), Variability of the behavior of the bottomside (B0, B1) parameters obtained from the ground-based ionograms at China's low latitude station, *Adv. Space Res.*, *42*, 695–702, doi:10.1016/j.asr.2007.07.022.